Chemical imaging beyond the diffraction limit using photothermal induced resonance microscopy

Andrea Centrone[1,2], Basudev Lahiri,[1,2] and Glenn Holland[1]*

[*] Dr. Andrea Centrone,
[1]Center for Nanoscale Science and Technology, National Institute of Standards and Technology, Gaithersburg, MD 20899 (USA)
[2]Maryland Nanocenter, University of Maryland, College Park, MD 20742 (USA) E-mail: Andrea.Centrone@nist.gov

Abstract: Photo Thermal Induced Resonance (PTIR), recently attracted great interest for enabling chemical identification and imaging with nanoscale resolution. In this paper, the PTIR working principles are reviewed along with the main results from a recent publication aimed at assessing the PTIR lateral resolution, sensitivity and linearity. For this purpose nano-patterned polymer samples were fabricated using electron beam lithography directly on 3-dimensional zinc selenide prisms. Results show that the PTIR lateral resolution for chemical imaging is comparable to the lateral resolution obtained in the AFM height images, up to the smallest feature measured (100 nm). Spectra and chemical maps were produced from the thinnest sample analyzed (40 nm). Notably, our experiments show that the PTIR signal increases linearly with thickness for samples up to ≈ 1 μm (linearity limit), a necessary requirement to use of the PTIR technique for quantitative chemical analysis at the nanoscale. Finally, the analysis of thicker samples provides evidence that the previously developed PTIR signal generation theory is correct. We believe that our findings will foster nanotechnology development in disparate applications by proving a basis for quantitative chemical analysis with nanoscale resolution.

Introduction

Nanomaterials attract great interest for their novel size-dependent properties, which outperform their macroscopic counterparts.[1-3] Investigation of nanomaterials' local properties

(chemical, physical, etc.) as a function of location is a prerequisite for their advanced engineering and application in fields like electronics,[4] photovoltaics,[5] biology,[6] and therapeutics.[1, 7] Typically, nanomaterials are characterized sequentially at the nanoscale with multiple imaging or spectroscopic techniques that give morphological, structural or chemical information at different length scales and/or sample locations. For example, Fourier Transform Infrared (FTIR) spectroscopy provides rich chemical and structural information,[6, 8] but the diffraction of the long infrared (IR) wavelengths (3 μm to 20 μm) limits the lateral resolution of FTIR microscopy to several micrometers.[9, 10] In contrast, Atomic Force Microscopy (AFM) is characterized by high lateral resolution but, per se, do not provide any information about the chemical nature of the sample. To circumvent these limitations a few chemical imaging methods combining scanning probe and spectroscopic techniques have been proposed.[11-13] However, relying on scanning probe techniques to extract physical or chemical quantities is often not straightforward.[14, 15]

For example, scattering Scanning Near-field Optical Microscopy (s-SNOM)[4, 11, 16] measures the light scattered by a sharp metallic tip in the near field when illuminated by a laser beam. In s-SNOM, nanoscale contrast can be obtained because the near field interaction of IR light with the sample induces a change in the amplitude and phase of the scattered light as a function of the (local) index of refraction ($\tilde{n}(\lambda)$) given by:

$$\tilde{n}(\lambda) = n(\lambda) + i\kappa(\lambda), \qquad (1)$$

where λ is the wavelength of light, n is the real part of the refractive index, and κ is the extinction coefficient. Since the s-SNOM signal is a complex function of κ (the relevant quantity in FTIR spectroscopy) and the scattered light depends on the tip-sample relative size[16] the interpretation of IR s-SNOM spectra relies on theoretical modeling.[14] s-SNOM modeling requires describing of the tip-sample-substrate interactions in the near field making the identification of unknown materials and the extraction of chemical information, a

challenging task. Recently, a new s-SNOM set up measuring both the amplitude and phase of the scattered light using an asymmetric Michelson interferometer allowed computing s-SNOM spectra that, in good approximation, resemble far field FTIR spectra.[17] However, for materials identification it would be advantageous obtaining IR spectra with a technique whose signal is a simple function of κ like the PTIR technique.

PTIR is a new technique that combines the high lateral resolution of Atomic Force Microscopy (AFM) and the high chemical specificity of IR Spectroscopy.[13, 18-21] PTIR spectra are obtained by measuring the instantaneous thermal expansion of the sample induced by the absorption of IR pulses with an AFM tip operating in contact mode (**Figure 1**). Unlike FTIR, in PTIR the lateral resolution for chemical imaging does not depend on the wavelength of light but depends on the tip size and on the sample's thermo-mechanical properties.[22, 23] PTIR has been used for nanoscale chemical characterization of inhomogeneous samples such as bacteria,[13, 19] polymers,[20] embedded quantum dots[24], inorganic nanoparticles[25] and even living cells.[26] In a recent paper[21] we have demonstrated that the PTIR signal is proportional to the absorbed energy, a necessary step towards the use of PTIR for nanoscale quantitative chemical characterization in many applications. Since the PTIR signal is sensitive only to absorption, not to scattering, the PTIR spectra can be used for materials identification via direct comparison of the recorded spectra with FTIR libraries.[20, 27]

In this article we review the major findings of our original work.[21] In particular, the lateral resolution, linearity and sensitivity of the PTIR technique is evaluated by measuring nano-patterned polymethylmethacrylate (PMMA) features fabricated on top of zinc selenide (ZnSe) prisms using electron beam lithography (EBL). Results shows that PTIR lateral resolution for chemical imaging is comparable to the lateral resolution obtained in the AFM height images, up to the smallest feature measured (100 nm). Spectra and chemical maps were produced from the thinnest sample analyzed (40 nm).[21] Additionally, we show that the PTIR spectral intensity of thin films (< 1 μm) depends linearly on the sample thickness which is a necessary

requirement to use PTIR spectra and images for quantitative analysis at the nanoscale.[21] Finally, by analyzing samples with an extended range of thicknesses we show experimentally that the PTIR signal intensity is proportional to the local energy absorbed, to the thermal expansion and to persistence time of the thermal excitation in the sample as previously predicted theoretically.[22, 23]

Materials and method

All chemicals were used as received without further purification.

PMMA resolution and wedge samples were fabricated using custom made adaptor pieces for a spinner and an EBL tool. The details of the nanofabrication process were described previously.[21]

The PTIR instrument used in this work uses an optical parametric oscillator (OPO) laser with 1 kHz repetition rate and wavelength output tunable between ≈ 1100 cm^{-1} and 4000 cm^{-1}. PTIR spectra were recorded by averaging 4 consecutive spectra in the range between 1200 cm^{-1} and 1800 cm^{-1}. Each individual spectrum was recorded tuning the laser at 3 cm^{-1} interval and using 256 pulses per wavelength. PTIR images were recorded using the laser at a fixed wavelength by averaging from 16 to 64 pulses per pixel.

A least square method was used to estimate the penetration depth (*dp*) values fitting the experimental data. The method employs an iterative strategy to minimize the deviations of the theoretical curve from the experimental points based on the Levenberg-Marquardt algorithm.

Results and Discussion

PTIR requires a tunable pulsed laser source for sample illumination and an AFM tip in contact mode to measure the instantaneous thermal expansion induced by light absorption in the sample. The typical setup takes advantage of a total internal reflection configuration for

illuminating the sample and minimizing the light-tip interaction. This requires placing the sample over an optically transparent prism (**Figure 1a**). As the laser wavelength is tuned to match the sample's IR vibrational absorptions, the sample heats-up, expands and deflects the AFM cantilever on a time scale much faster than the response of the AFM feedback. The instantaneous tip deflection is measured using a four-quadrant detector **(Figure 1a)** and the low repetition of the laser pulses (1 kHz) assures that the cantilever has enough time to complete the ring-down **(Figure 1b).** Consequently, a new pulse will excite a sample and cantilever that have returned to equilibrium. The sample PTIR spectrum is obtained by plotting the amplitude of the tip deflection as a function of frequency. The analysis of the PTIR signal is carried out either by determining the maximum of the deflection during the cantilever ring down **(Figure 1b)** or by determining the amplitude of one of the cantilever normal modes obtained by the Fourier transformation of the ring down signal **(Figure 1c)**. Typically several pulses are averaged at each wavelength to increase the signal to noise ratio. Chemical images can be obtained by illuminating the sample at a constant wavelength while scanning the AFM tip.[19, 21, 28] In order to record a chemical image with the best lateral resolution,[21] the pixel acquisition rate for the AFM (ξ_{AFM}) should equal that of PTIR (ξ_{PTIR}) defined as follows:

$$\xi_{AFM} = 2 \cdot n^{pixel} \cdot \nu \tag{2}$$

$$\xi_{PTIR} = \frac{\omega}{n^{avg-pulses}} \tag{3}$$

where n^{pixel} (pixel/line) is the number of pixel in the AFM scanning direction, v is the AFM scan rate per line (s^{-1}), ω is the laser repetition rate (1 kHz in this work) and $n^{avg\text{-}pulses}$ is the number of pulses per pixel (typically from 16 to 64). If this condition is not met the pixel size of the PTIR chemical image will differ from the pixel size in the height image making correlations difficult if the two numbers are appreciably different.

A sample made of PMMA and Polystyrene (PS) particles embedded in an epoxy matrix is used here to illustrate the chemical specificity of the PTIR signal. While the AFM height image alone **(Figure 2a)** doesn't allow phase identification, PTIR chemical image **(Figure 2b)** and spectra **(Figure 2c)** unambiguously identify the composition of the different phases[21, 25] The AFM height image and the PTIR chemical images in **Figure 2** were acquired simultaneously while illuminating the sample with the laser set at 1721 cm^{-1}, characteristic of the PMMA carbonyl groups,[29] but not absorbed by PS or by epoxy . Clearly the AFM height and the PTIR images carry different information (topography and chemical information, respectively).

The samples studied here can be grouped into 2 categories: samples with constant thickness patterned with various features size and spacing (hereafter, resolution samples) used to assess the PTIR lateral resolution and samples with variable height patterned with lines (hereafter, wedged samples) to assess PTIR sensitivity and linearity.

The samples nanofabrication process is illustrated in **Figure 3**. Briefly, a PMMA positive EBL resist was spun on a prism using a custom adaptor piece[21] and cured before depositing an aluminum charge dissipation layer. Using another custom adaptor piece,[21] the prism was then subjected to EBL varying the electron beam dose depending on the type of pattern required. Finally, the aluminum layer was removed with a tetramethylammonium hydroxide water solution and the pattern was developed in a mixture of methyl-iso-butylketone and isopropyl alcohol. Depending on the electron beam dose the PMMA film was patterned through the whole thickness (**Figure 3e**) or partially (**Figure 3f**). PMMA wedged samples were prepared with a very similar process by spinning the prisms at an angle. Details of the nanofabrication process are reported in our original publication.[21]

The AFM height image and the corresponding PTIR image of PMMA carbonyl groups (1720 cm^{-1}) of an EBL defined resolution sample are compared in **Figure 4**. The thickness of

PMMA is 290 nm ± 10 nm while the patterned features are ≈ 85 nm tall. The contrast in figure 4b is given by differences in the absorption intensity due to different sample thickness between the top (≈ 290 nm) and bottom (≈ 205 nm) of the lithographically defined features. The images were acquired with 25 nm pixel resolution and 64 pulses were averaged for each pixel. The correlation between the AFM height and the PTIR images (amplitude and peak) for the resolution samples is generally very good and the lateral resolution in the images is comparable within the experimental limits (± 10 nm), see Figure 4. The smallest feature measured in our original work was ≈ 100 nm as determined from both the height and chemical images.[21] The ultimate lateral resolution of the PTIR technique lies below 100 nm but it could not be determined with the samples described here. PTIR images and spectra were obtained from a sample as thin as 40 nm ± 5 nm (the thinnest sample analyzed).[21]

PTIR spectra obtained on patterned wedged samples with variable PMMA thickness **(Figure 5a)** were used to evaluate the linearity and sensitivity of the technique and to determine experimentally the dependence of the PTIR signal on sample thickness and optical constants. These experiments demonstrate that the PTIR signal is proportional to the energy absorbed (see below). **Figure 5b** shows that the PTIR signal increases linearly with thickness (z) for thicknesses up to ≈ 1 μm.[21] As the thickness is increased the PTIR signal reaches a maximum, which is wavelength dependent, and then progressively decreases (**Figure 5c**) due to the exponentially decaying field inside the sample caused by the attenuated total reflection (ATR) illumination geometry. Below we show a simple model that describes well the PTIR signal trend as a function of thickness.

Dazzi et al. derived theoretically a complex expression for the PTIR signal.[22, 23] In short, the PTIR signal is expected to be proportional to the sample thermal expansion, to the absorbed energy per unit area (U_{abs}) and, for short laser pulses, to the duration of the thermal excitation (t_{relax}) in the sample. The sample thermal expansion is proportional to the sample thickness (z)

while t_{relax} is approximately proportional to square of the sample thickness.[22] Consequently, it is expected that the PTIR signal (S) should be proportional to:

$$S \sim U_{abs} \cdot z^3 \quad (4)$$

The ATR configuration and sample thicknesses used in this work combined with the relatively strong absorption of PMMA[30] cause the sample absorption to be a function of the evanescent electric field intensity. In ATR spectroscopy[31] it is convenient to express the exponentially decaying evanescent field amplitude inside the sample in terms of penetration depth (d_p)

$$E = E_0 \cdot e^{-z/d_p} \quad (5)$$

Where E_0 is the electric field amplitude at the prism interface and d_p is the distance where E is reduced by a factor of e. It should be noted that the actual thickness sampled by the evanescent field is greater than d_p. The penetration depth depends on the wavelength (λ), the indexes of refraction of the not-absorbing ATR element (n_1) and of the sample ($\tilde{n}_2(\lambda) = n_2(\lambda) + i\kappa_2(\lambda)$) and the light angle of incidence (θ):

$$d_p = \frac{\lambda}{2 \cdot \pi} \cdot \left[\frac{\sqrt{\left(n_1^2 \cdot sin^2\theta - n_2^2 + k_2^2\right)^2 + \left(2 \cdot n_2 \cdot k_2\right)^2} + \left(n_1^2 \cdot sin^2\theta - n_2^2 + k_2^2\right)}{2} \right]^{-1/2} \quad (6)$$

Both the real part and the imaginary part of the refractive index change as a function of λ in proximity of the PMMA absorption peaks[30] The experimental conditions used here (θ = 45°, n_1 = 2.438, $n2(\lambda)$ = 1.2 to 1.65, $k_2(\lambda)$ = 0 to 0.4)[30] ensure that total internal reflection is achieved at all wavelengths (from 1800 cm^{-1} to 1200 cm^{-1}) at the prism-sample interface.

For non-absorbing samples the expression of d_p is reduced to

$$d_p(k_2 = 0) = \frac{\lambda}{2 \cdot \pi \cdot n_1} \cdot \left[sin^2\,\theta - \left(\frac{n_2}{n_1}\right)^2 \right]^{-1/2} \quad (7)$$

Because of the conservation of energy we can express the absorbed energy per unit area by a sample as the difference between the evanescent field intensities calculated for a non-absorbing medium and for a sample with extinction coefficient κ_2:

$$U_{abs} \sim E^2_{k=0} - E^2_{k=k2} \quad (8)$$

which is a non-monotonic function of *z* (**Figure 5d**).[21] The experimental data fit well when substituting equation 8 into equation 4 (see **Figure 5c**). The penetration depth calculated by fitting the experimental data increases with wavelength as expected and was determined to be 1070 nm ± 9 nm, 1113 nm ± 12 nm and 1160 nm ± 9 nm for the PMMA absorption peak at 1720 cm^{-1}, 1463 cm^{-1} and 1263 cm^{-1}, respectively.[21] Our experiments prove that the PTIR theory developed by Dazzi et al.[23] is fundamentally correct.

The linearity of the PTIR signal with thickness (**Figure 5b**) suggests that PTIR data could potentially be used for quantitative chemical analysis at the nanoscale for thin samples (z smaller than ≈ 1 μm). For this purpose one should link the PTIR signal to the concentration (*C*). Since the PTIR signal is proportional to the absorbed energy and, under the conditions of validity of the Lambert and Beer approximation, the absorbance of a sample is proportional to its concentration, one should expect the PTIR signal to be proportional to the concentration. This assumption is valid for a mixture in which the components have the same thermo-mechanical parameters, but a deviation from linearity is expected if the components have significantly different thermo-mechanical properties. However, for mixtures of materials with similar thermo-mechanical properties such as some biological samples, polymers blends and diluted mixtures we expect this deviation to be small.[21]

3. Conclusions

In summary, the limits of PTIR technique were tested by analyzing nano-patterned polymer samples fabricated on unconventional 3-diemnsional substrates. It was found it that PTIR is a robust tool for simultaneous extraction of topological and chemical maps at the nanoscale. We have used a simple model and experimentally demonstrated that the PTIR signal is proportional to the energy absorbed and that the theory of PTIR signal generation[23] is correct. Arguably, the most important finding of our work is that for thin samples (z smaller than ≈ 1 μm) the PTIR signal increases linearly as a function of sample thicknesses. This means that PTIR data could potentially be used for quantitative chemical analysis at the nanoscale impacting areas from material science to biology and medicine.

Acknowledgements

The authors acknowledge Dr. Adrian Popescu of NIST for the help in fitting the data, Rich Kasica of NIST for useful discussion of EBL and Kevin Kjoller of Anasys Instruments for providing the microtomed sample. A. C. acknowledges support from the National Institute of Standards and Technology American Recovery and Reinvestment Act Measurement Science and Engineering Fellowship Program, Award 70NANB10H026, through the University of Maryland. A. C. and B. L. acknowledge support under the Cooperative Research Agreement between the University of Maryland and the National Institute of Standards and Technology Center for Nanoscale Science and Technology, Award 70NANB10H193, through the University of Maryland.

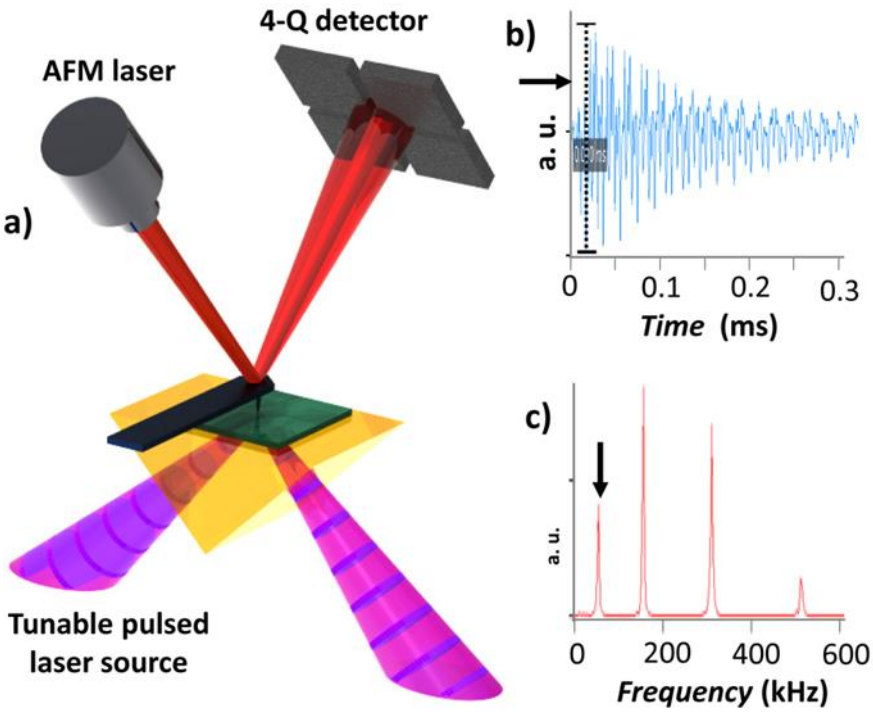

Figure 1. a) Schematic of the PTIR set up: if the IR laser pulses (purple) are absorbed by the sample (green) it rapidly expands and deflects the AFM cantilever; the amplitude of the deflection, which is proportional to the energy absorbed, is measured by the AFM four-quadrant detector. The PTIR signal analysis is carried out either by (b) determining the maximum of peak to peak deflection during the cantilever ring down (blue signal) or by (c) Fourier transformation determining the amplitude of one of the cantilever normal modes of vibration (red signal). The image was adapted from Lahiri B. et al.[21]

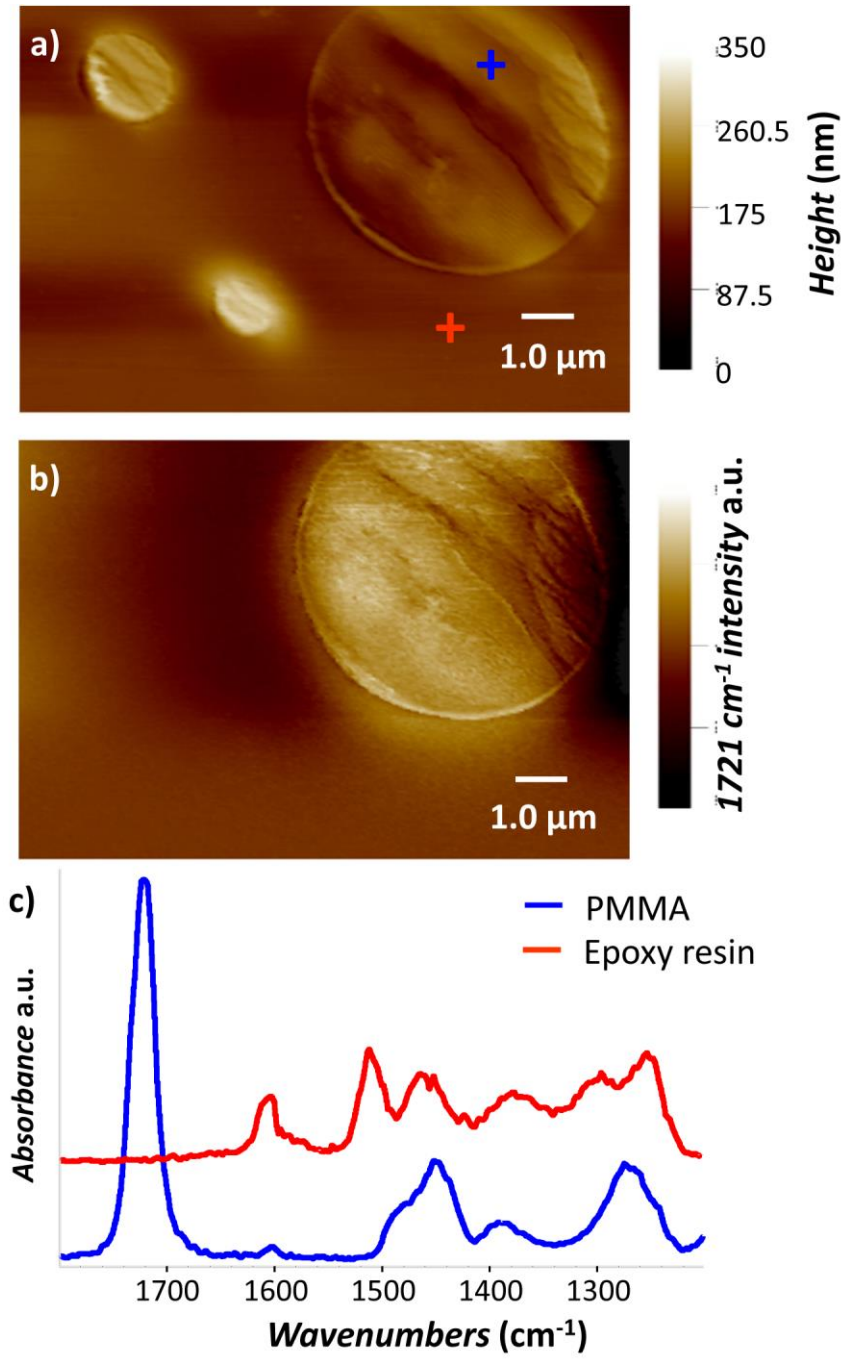

Figure 2. a) AFM height image showing a PMMA particle (large) and 2 PS particles (small) embedded in epoxy resin, b) simultaneous PTIR chemical image obtained pulsing the IR laser at 1721 cm^{-1} a frequency characteristic of the carboxylic groups of PMMA; the PTIR image allows to identify the chemical composition of the different phases in the sample. c) PTIR spectra of PMMA (blue) and epoxy resin (red) obtained from the selected locations (red and blue +) in fig. 2a. The image was adapted from Lahiri B. et al.[21]

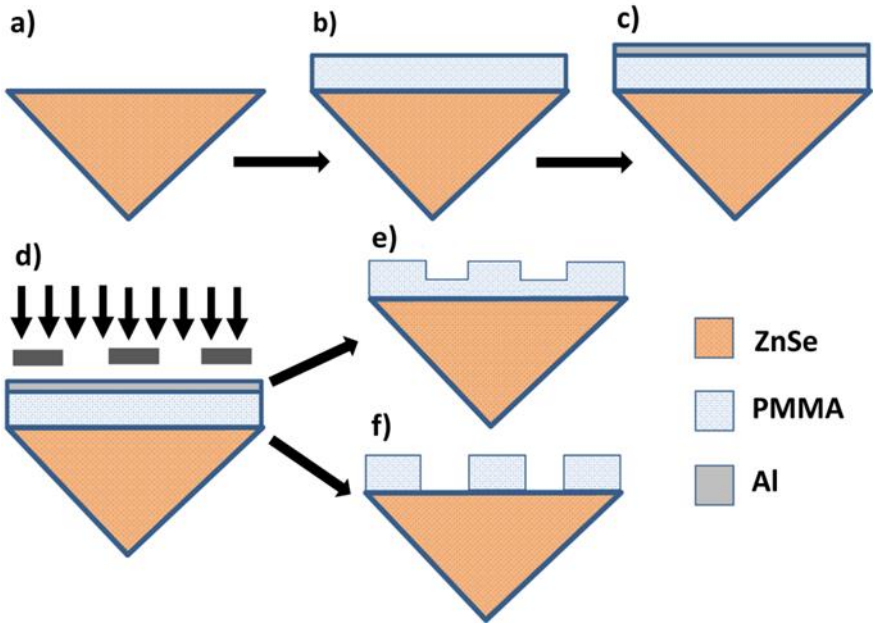

Figure 3. Nanofabrication schematic of PMMA resolution samples on ZnSe prisms: a) prism cleaning, b) PMMA spinning, c) aluminum charge dissipation layer deposition, d) Electron Beam Lithography process, e, f) aluminum layer removal and PMMA development; the height of the patterned features is a function of the electron beam dose used. The image was adapted from Lahiri B. et al.[21]

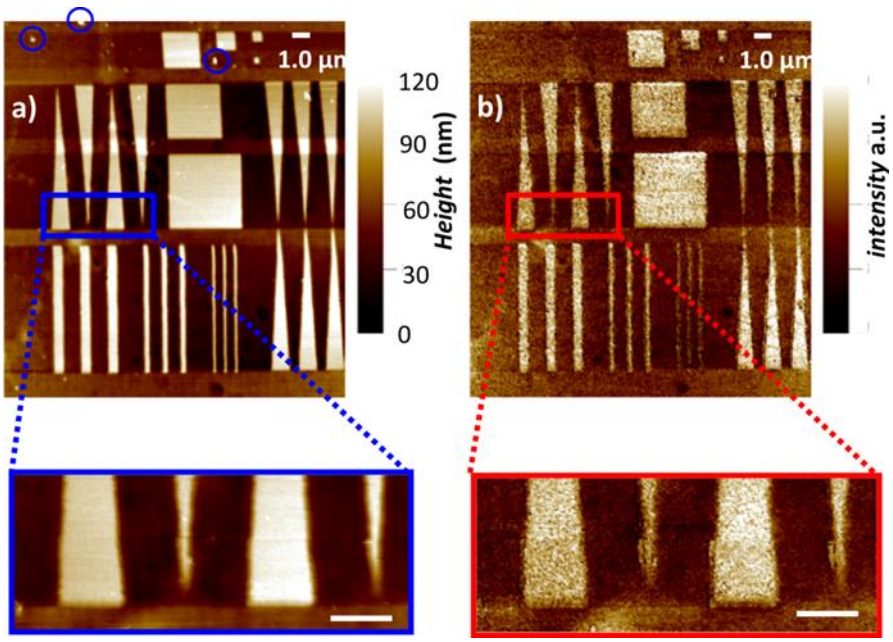

Figure 4. PMMA patterned sample: a) AFM height image, b) PTIR chemical image (amplitude signal) recorded by pulsing the IR laser at 1720 cm^{-1} characteristic of the PMMA carbonyl groups. The scale bar in the insets is 1 µm. A few small features (attributed to dust particles extraneous to the sample) observed in the height image (blue circles) but don't appear in the chemical image. The image was adapted from Lahiri B. et al.[21]

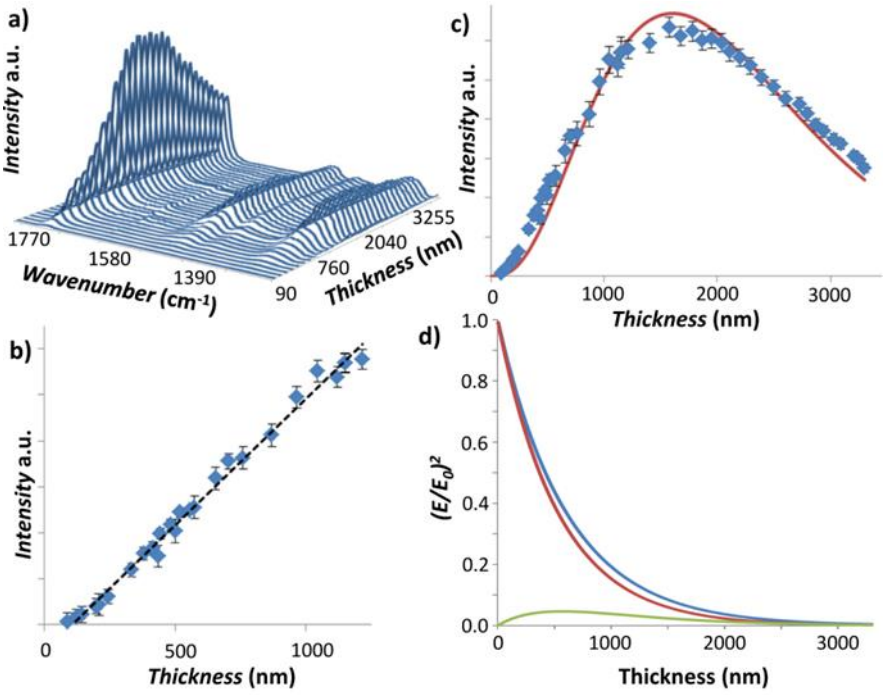

Figure 5. a) PTIR spectra intensity of PMMA as a function of thickness. b) Intensity of the 1720 cm^{-1} PMMA peak as a function of thickness; linear interpolation has a correlation coefficient (R2) of 0.993 for thicknesses up to 1200 nm. c) Intensity of the 1720 cm^{-1} PMMA peak as a function of thickness for thicknesses up to 3300 nm; experimental data are interpolated by the function $a \cdot z^3 \cdot e^{-2 \cdot \frac{z}{dp}}$ with R^2=0.963 and dp=1070 nm ± 9 nm. d) Calculated evanescent electric field intensity (λ = 1720 cm^{-1}, θ = 45° and n_{ZnSe} = 2.438 in the case of a not absorbing medium (blue, n_{PMMA} = 1.54, k_2 = 0) and in the case of PMMA (red, n_{PMMA} = 1.54, k_{PMMA} = 0.2). The calculated absorbed energy as a function of thickness according equation 8 is shown in green. The horizontal error bars, which are smaller than the dots size, represent a single standard deviation in the AFM height measure. The vertical error bars represent a single standard deviation in the integration of the PTIR lines. The image was adapted from Lahiri B. et al.[21]

1. Zhang, L.J. & Webster, T.J. Nanotechnology and nanomaterials: Promises for improved tissue regeneration. *Nano Today* **4**, 66-80 (2009).
2. Centrone, A. et al. The role of nanostructure in the wetting behavior of mixed-monolayer-protected metal nanoparticles. *Proceedings Of The National Academy Of Sciences Of The United States Of America* **105**, 9886-9891 (2008).
3. El-Sayed, M.A. Some interesting properties of metals confined in time and nanometer space of different shapes. *Accounts Of Chemical Research* **34**, 257-264 (2001).
4. Huber, A.J., Wittborn, J. & Hillenbrand, R. Infrared spectroscopic near-field mapping of single nanotransistors. *Nanotechnology* **21**, 235702 (2010).
5. Nicholson, P.G. & Castro, F.A. Organic photovoltaics: principles and techniques for nanometre scale characterization. *Nanotechnology* **21**, 492001 (2010).
6. Fernandez, D.C., Bhargava, R., Hewitt, S.M. & Levin, I.W. Infrared spectroscopic imaging for histopathologic recognition. *Nature Biotechnology* **23**, 469-474 (2005).
7. Park, J.H. et al. Cooperative Nanoparticles for Tumor Detection and Photothermally Triggered Drug Delivery. *Advanced Materials* **22**, 880-885 (2009).
8. Centrone, A., Hu, Y., Jackson, A.M., Zerbi, G. & Stellacci, F. Phase separation on mixed-monolayer-protected metal nanoparticles: A study by infrared spectroscopy and scanning tunneling microscopy. *Small* **3**, 814-817 (2007).
9. Petibois, C., Piccinini, M., Guidi, M.C. & Marcelli, A. Facing the challenge of biosample imaging by FTIR with a synchrotron radiation source. *Journal of Synchrotron Radiation* **17**, 1-11 (2010).
10. Nasse, M.J. et al. High-resolution Fourier-transform infrared chemical imaging with multiple synchrotron beams. *Nature Methods* **8**, 413-U458 (2011).

11. Knoll, B. & Keilmann, F. Near-field probing of vibrational absorption for chemical microscopy. *Nature* **399**, 134-137 (1999).
12. Bozec, L. et al. Localized photothermal infrared spectroscopy using a proximal probe. *Journal of Applied Physics* **90**, 5159-5165 (2001).
13. Dazzi, A., Prazeres, R., Glotin, F. & Ortega, J.M. Analysis of nano-chemical mapping performed by an AFM-based ("AFMIR") acousto-optic technique. *Ultramicroscopy* **107**, 1194-1200 (2007).
14. Cvitkovic, A., Ocelic, N. & Hillenbrand, R. Analytical model for quantitative prediction of material contrasts in scattering-type near-field optical microscopy. *Optics Express* **15**, 8550-8565 (2007).
15. Fischer, H. Quantitative determination of heat conductivities by scanning thermal microscopy. *Thermochimica Acta* **425**, 69-74 (2005).
16. Brehm, M., Taubner, T., Hillenbrand, R. & Keilmann, F. Infrared spectroscopic mapping of single nanoparticles and viruses at nanoscale resolution. *Nano Letters* **6**, 1307-1310 (2006).
17. Huth, F. et al. Nano-FTIR Absorption Spectroscopy of Molecular Fingerprints at 20 nm Spatial Resolution. *Nano Letters* **12**, 3973-3978 (2012).
18. Dazzi, A., Prazeres, R., Glotin, E. & Ortega, J.M. Local infrared microspectroscopy with subwavelength spatial resolution with an atomic force microscope tip used as a photothermal sensor. *Optics Letters* **30**, 2388-2390 (2005).
19. Dazzi, A. et al. Chemical mapping of the distribution of viruses into infected bacteria with a photothermal method. *Ultramicroscopy* **108**, 635-641 (2008).
20. Marcott, C., Lo, M., Kjoller, K., Prater, C. & Noda, I. Spatial Differentiation of Sub-Micrometer Domains in a Poly(hydroxyalkanoate) Copolymer Using Instrumentation that Combines Atomic Force Microscopy (AFM) and Infrared (IR) Spectroscopy. *Applied Spectroscopy* **65**, 1145-1150 (2011).
21. Lahiri, B., Holland, G. & Centrone, A. Chemical Imaging Beyond the Diffraction Limit: Experimental Validation of the PTIR Technique. *Small* **9**, 439-445 (2013).
22. Dazzi, A. in Thermal Nanosystems and Nanomaterials, Vol. 118. (ed. S. Volz) 469-503 (2009).
23. Dazzi, A., Glotin, F. & Carminati, R. Theory of infrared nanospectroscopy by photothermal induced resonance. *Journal of Applied Physics* **107**, 124519 (2010).
24. Sauvage, S. et al. Homogeneous broadening of the S to P transition in InGaAs/GaAs quantum dots measured by infrared absorption imaging with nanoscale resolution. *Physical Review B* **83**, 035302 (2011).
25. Katzenmeyer, A.M., Aksyuk, V. & Centrone, A. Nanoscale Infrared Spectroscopy: Improving the Spectral Range of the Photothermal Induced Resonance Technique. *Analytical Chemistry* **85**, 1972-1979 (2013).
26. Mayet, C. et al. Sub-100 nm IR spectromicroscopy of living cells. *Optics Letters* **33**, 1611-1613 (2008).
27. Kjoller, K., Felts, J.R., Cook, D., Prater, C.B. & King, W.P. High-sensitivity nanometer-scale infrared spectroscopy using a contact mode microcantilever with an internal resonator paddle. *Nanotechnology* **21**, 185705 (2010).
28. Felts, J.R., Kjoller, K., Lo, M., Prater, C.B. & King, W.P. Nanometer-Scale Infrared Spectroscopy of Heterogeneous Polymer Nanostructures Fabricated by Tip-Based Nanofabrication. *Acs Nano* **6**, 8015-8021 (2012).
29. Bellamy, L.J. The Infrared Spectra of Complex Molecules, Edn. second. (New York; 1980).
30. Graf, R.T., Koenig, J.L. & Ishida, H. OPTICAL-CONSTANT DETERMINATION OF THIN POLYMER-FILMS IN THE INFRARED. *Applied Spectroscopy* **39**, 405-408 (1985).

31. Harrick, N.J. Internal Reflection Spectroscopy. (Interscience Pubblisher, New York; 1967).